

Stony Brook University



OFFICIAL COPY

The official electronic file of this thesis or dissertation is maintained by the University Libraries on behalf of The Graduate School at Stony Brook University.

© All Rights Reserved by Author.

Structural Study of INO80 Chromatin Remodeling Protein Complex by Cryo-EM

A Thesis Presented

by

Won Kyun Koh

to

The Graduate School

in Partial Fulfillment of the

Requirements

for the Degree of

Master of Science

in

Biochemistry and Cell Biology

Stony Brook University

December 2013

Stony Brook University

The Graduate School

Won Kyun Koh

We, the thesis committee for the above candidate for the
Master of Science degree, hereby recommend
acceptance of this thesis.

Huilin Li, Ph.D. – Thesis Advisor
Professor, Department of Biochemistry and Cell Biology

Ed Luk, Ph.D. – Second Reader
Assistant Professor, Department of Biochemistry and Cell Biology

This thesis is accepted by the Graduate School

Charles Taber
Dean of the Graduate School

Abstract of the Thesis

Structural Study of INO80 Chromatin Remodeling Protein Complex by Cryo-EM

by

Won Kyun Koh

Master of Science

in

Biochemistry and Cell Biology

Stony Brook University

2013

The human genome, comprised of ~three billion base pairs, is over six feet long when fully extended. Multiple chromatin modifying enzymes are required either to condense the DNA to fit into each nucleus that are ~ 1 μ m in size, or to partially unravel the chromatin for readout of the genomic information. The ATP-dependent chromatin remodeler INO80 plays important roles in regulating the spacing of nucleosomes along the DNA. However, mechanism by which INO80 slides the nucleosome is still unclear. Structural studies of other chromatin remodelers have been shown to be a powerful approach to understand how these enzymes interact with and modulate the positioning of nucleosome. Although X-ray crystallography can provide high resolution structure, it is not appropriate for studying INO80 because INO80 is a large protein complex (~1.3MDa) consisted of multiple subunits and modules, and only a small quantity of the protein complex can be purified. Electron microscopy (EM) is well suited for structural analysis of INO80 given the large molecular weight of the complex and the proven success of the EM approach in solving the structure of other remodelers. In this study, we used EM to study the structure and conformation range of the INO80 complex. We generated 3D class averages and 3D models of the INO80 complex based on data obtained from cryo-EM and negative stained EM. We found that INO80 is a bipartite structure with a rigid head region and an extended highly flexible tail region. The head region is a donut-shaped-structure containing the potential ATPase Rvb1/2 hexamer. On the basis of the structural features, we propose that INO80 may mediate ATP-dependent nucleosome sliding while wrapping its tail around the nucleosome.

Dedication Page

I dedicate my work to my family.

Table of Contents

List of Figures	vi
List of Abbreviations	vii
Acknowledgements	ix
I. Introduction	1
ATP Dependent Chromatin Remodelers	2
The Mechanism of Histone Octamer Sliding	2
INO80	3
a. INO80 Components and Interactions	3
b. INO80 Subunits	4
b.1 Ino80	4
b.2 Actin and ARP	5
b.3 Rvb1/2	5
b.4 Other Subunits	7
EM Approach to Studying INO80 Structure	7
a. EM Sample Preparation	8
b. Chemical Fixation	9
c. Image Alignment	9
d. 2D Classification and 3D Reconstruction	10
II. Materials and Methods	11
Sample Preparation	11
Grid Preparation	11
Sample on Grid	11
EM Imaging	11
2D Classification and 3D Reconstruction	12
III. Results	13
WT INO80	13
INO80 with MBP Labeled Subunits	15
INO80 bound to Nucleosome	17
IV. Discussion and Future Perspective	19
V. Supplemental Data	20
References	22

List of Figures

Figure 1: A diagram of eukaryotic DNA packaging	1
Figure 2: The Loop propagation model	3
Figure 3: A schematic representation of INO80 organization	4
Figure 4: Rvb1/2 structures	7
Figure 5: Examples of how CTF demonstrates EM image quality.....	8
Figure 6: The GraFix method	9
Figure 7: 2D class averages of WT INO80	14
Figure 8: WT INO80 3D models	15
Figure 9: NS-EM 2D class averages of INO80 with Rvb1-MBP	16
Figure 10: NS-EM 2D class averages of INO80 with Arp5-MBP	17
Figure 11: NS-EM 2D class averages of INO80 bound to nucleosome prepared with formaldehyde	18
Figure S1: “Embryo-Shaped” INO80 EM maps	20
Figure S2: Superposition of cryo-EM 3D maps of WT INO80 and Rvb1/2 dodecamer ring	21
Figure S3: Biochemical data to verify INO80 subunits and function	21

List of Abbreviations

NCP	Nucleosome Core Particle
TSS	Transcription Start Site
DSB	Double Strand Break
NFR	Nucleosome Free Region
SWI/SNF	Switch defective/Sucrose Nonfermenting
ISWI	Imitation Switch
Min2/CHD	Mitchell autoimmune antibodies 2/Chromodomain Helicase DNA binding
Chromodomain	Chromatin Organization Modifier Domain
INO80	Inositol-requiring 80
SWR1	SWI/SNF-related SWR1 complex
SNF2	Sucrose NonFermenting 2
SF2	Superfamily 2
Act1	Actin 1
Arp	Actin Related Protein
Rvb1/2	RuvB-like 1 /2
AAA+	ATPases Associated with diverse cellular Activities
Taf14	TBP-associated factor 14
Nhp10	Non-Histone Protein 10
HMG domain	High Mobility Group domain
Ies1-6	Ino Eighty Subunit 1-6
HSA	Helicase-SANT-Associated
SANT	Swi3, Ada2, N-Cor, and TFIIB
PAPA-1	PAP-1 Associated Protein
MBP	Maltose Binding Protein

MNase	Micrococcal Nuclease
DNase	Deoxyribonuclease
CX-MS	Conversion X-Ray Mossbauer Spectroscopy
XL-MS	Chemical Crosslinking and Mass Spectrometry
TEM	Transmission Electron Microscopy
FEG	Field Emission Gun
CCD	Charge Coupled Device
CTF	Contrast Transfer Function
GraFix method	Gradient Fixation method
AR	Angular Reconstruction
RCT	Random Conical Tilt
OTR	Orthogonal Tilt Reconstruction
SSNR	Spectral Signal to Noise Ratio
FT	Fourier Transform
MSA	Multivariate Statistical Analysis
FSC	Fourier Shell Correlation

Acknowledgments

I would like to thank Dr. Huilin Li for his generosity to provide an opportunity to join his lab to conduct this study. His unlimited support and encouragement allowed me to enjoy and explore my research with different approaches. He also revised the thesis writing. I like to thank Dr. Jingchuan Sun for technical guidance and support. He trained me for EM grid preparation, EM operation, and EM image processing. His dedication towards research has inspired me to become a better scientist. I would like to thank Dr. Lihong Wan for preparing INO80 sample for EM imaging. She also allowed me to observe sample preparation process and provided biochemical data. And I would like to thank Dr. Ed Luk for providing reading materials to understand about function of INO80 and numerous help for thesis writing. He also taught me how to think critically and present my opinion effectively.

I. Introduction

Human DNA wraps around the histone octamer to form the basic unit called nucleosome. Nucleosomes can stack on top of each other to form a higher order structure called the 30-nm fiber. These fibers can further condense by looping into a structure that is called the chromatid (**Fig. 1**). A nucleosome core particle (NCP) is consisted of 147 bp of double stranded DNA left-handedly coiled 1.65 turns around a central histone core (Bowman, 2010). The histone core is made up of two copies of each H2A, H2B, H3, and H4 histones which are organized into pairs of heterodimers: H2A-H2B and H3-H4. These 4 dimers are arranged about a 2-fold symmetry axis, called a dyad. Nucleosomes are organized along the DNA in an average periodicity of 165 bp in yeast and 185 bp in humans (Jiang and Pugh, 2009). This structure generally inhibits transcription. Mutations that perturb the density and the spacing of nucleosomes could lead to aberrant transcription (Han and Grunstein, 1988; Whitehouse et al., 2007). At the promoter of most genes, there is an 80-200 bp nucleosome free region (NFR), which is the site for the assembly of the transcription machinery as well as for the recruitment of chromatin remodeling factors. Flanking the NFR are well-positioned nucleosomes at the so called -1 and +1 positions. The +1 nucleosome blocks the transcription start site (TSS) and must be removed before the transcriptional open complex can assemble.

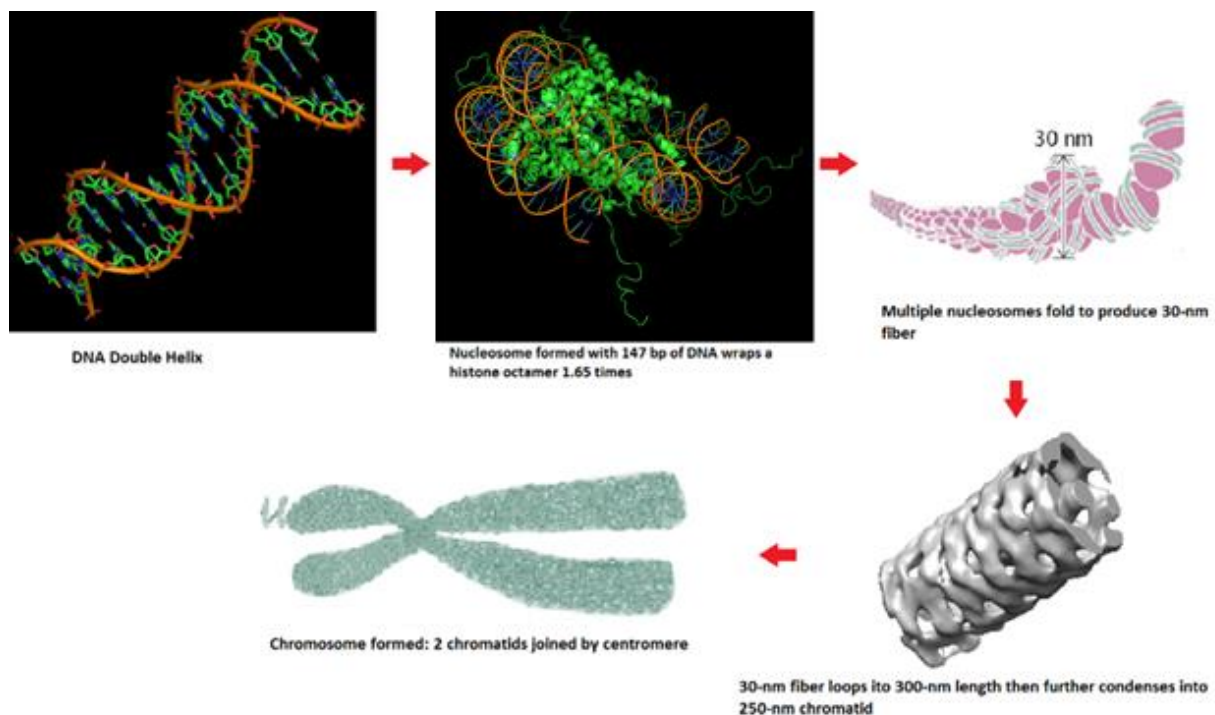


Figure 1. A diagram of eukaryotic DNA packaging. Simplified illustration shows how eukaryotic double stranded DNA folds into a chromosome through a hierarchical order.

ATP Dependent Chromatin Remodelers

A key question related to my research project is to understand how the regular spacing of the nucleosomes is established. ATP-dependent chromatin remodelers are known to be key players in this process (Rando and Winston, 2012). There are four major chromatin remodeler families in eukaryotes, namely SWI/SNF, ISWI, Min2/CHD, and INO80 (Rando and Winston, 2012). All members of these remodelers are multi-subunit complexes that contain a core ATPase, which is homologous to the SF2 DNA translocase domain. These enzymes are known to catalyze three types of remodeling reactions: 1) histone octamer sliding, 2) histone eviction and deposition, and 3) histone replacement (Clapier and Cairns, 2009). In my thesis, I will focus on the octamer sliding activity of the INO80 complex.

In vivo, the activity of octamer sliding is thought to play an important role in establishing the regular spacing of nucleosomes. When recombinant histone octamers were mixed with genomic DNA *in vivo*, they assembled into nucleosomes that were largely randomly positioned (Zhang et al., 2011b). However, the nucleosomes became organized to the periodic structure, when nuclear extracts and ATP were added, suggesting that enzymes such as the ATP-dependent remodelers might play a role. Consistent with this idea, inactivation of remodelers such as ISW1, ISW2, RSC, or CHD1 led to shift in nucleosomal positions either toward or away from the NFR. These observations have led to a model in which the remodelers “push” or “pull” histone octamer in opposite directions to establish the steady-state nucleosome architecture. Unpublished data from the Luk lab has shown that inactivation of INO80 causes nucleosomes to slide toward the NFR, suggesting that the *in vivo* function of INO80 is to push octamer away from the NFR.

The Mechanism of Histone Octamer Sliding

The goal of this study is to understand the mechanism of INO80 in sliding histone octamers along DNA. Studies from other chromatin remodelers (e.g. ISW1 and SWI/SNF) have led to the loop propagation model (**Fig. 2**). In this model, the histone octamer is bound by the DNA via interaction with the 14 points on the DNA minor grooves. Three of the 14 interactions are strong. The strong interactions are located near the dyad and 45-60 bp away from both sides of dyad. The ATPase translocase domain of the remodeler acts as a motor to slightly twist the DNA at the weaker contacts first, thereby promoting dissociation of one of the non-dyad contacts near the proximal linker end. As a result a loop is created (Bowman, 2010). This loop propagates toward the distal linker, disrupting DNA-histone octamer interactions in the front and reforming them behind. Repeated actions cause DNA to slide.

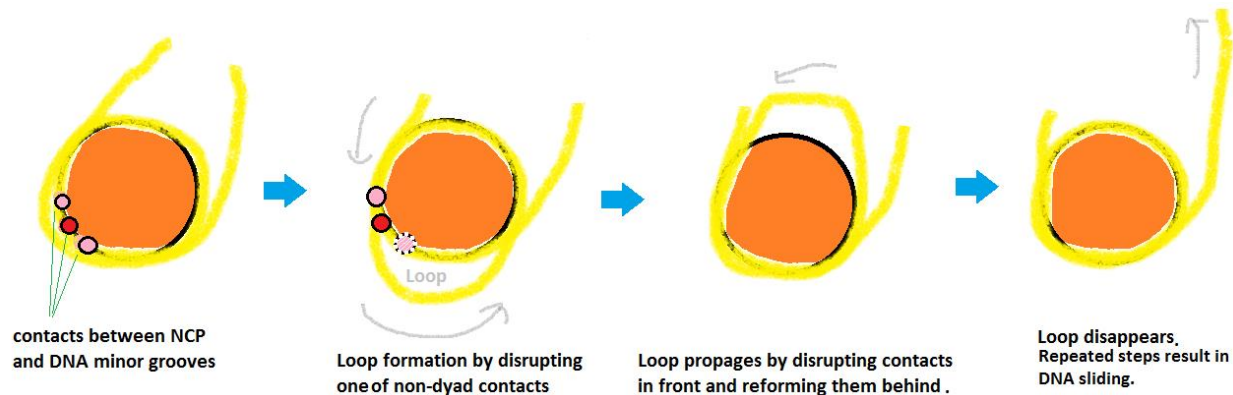


Figure 2. The Loop propagation model. A NCP slides on DNA by forming a loop which disrupts histone-DNA contacts. First, ATPase traslocase domain of the remodeler twists DNA at weaker contacts (pink dots) which leads to loop formation. Histone octamer-DNA interactions in the front disrupt and reform behind as the loop propagates toward distal linker. (Bowman, 2010).

INO80

The multi-subunit INO80 complex (which will be referred to as INO80 hereafter) is a member of the ATP-dependent chromatin remodeler families. INO80 was proposed to play several roles in various biological functions including DNA transcription, DNA replication, and DNA repair (Conaway and Conaway, 2009). INO80 catalyzes nucleosome sliding away from promoter. However, it is not known whether a similar loop propagation mechanism (**Fig. 2**) is also true for INO80. In yeast, INO80 is involved in replication fork progression under genotoxic stress (Clapier and Cairns, 2009). One of the subunits of INO80, Arp4 is shown to recognize the phosphorylated Ser129 at the C-terminal region of H2A; such modification is often associated with regions near DNA repair site (Conaway and Conaway, 2009). INO80 is also involved in exposing DNA near the DSB and overcoming cell-cycle arrest (Morrison and Shen, 2009).

a. INO80 Components and Interactions

The *S. cerevisiae* INO80 has a molecular mass of approximately 1.3 MDa and it is composed of 15 different subunits: Ino80 (which is the largest subunit of INO80), Act1, Arp 4,5,8, Rvb1/2, Taf14, Nhp10, and Ies 1-6. Nine subunits of INO80 are conserved from yeast to human: Ino80, Act1, Arp 4,5,8, Rvb1/2, and Ies2,6 (Jin et al., 2005). Some of the subunits of INO80 are shared by other chromatin remodelers. For example, Act1, Arp4, and Rvb1/2 are found in other member of the INO80 subfamily remodeler SWR1 (Clapier and Cairns, 2009). Biochemical studies have revealed the hierarchy of subunit organization of INO80 (**Fig. 3**) (Tosi et al., 2013; Watanabe and Peterson, 2010). For example, deletion of Arp8 led to loss of Arp4 and Act1 suggesting these proteins form a subdomain (Shen et al., 2003). Furthermore, conditional depletion of the Rvb1 and Rvb2 subunits led to dissociation of the Arp5 subunit, thus placing these subunits close together within complex (Jónsson et al., 2004). Finally, a recent crosslinking-coupled mass spectrometry technique reviewed that the subunits are organized in four independent modules in INO80 with Ino80-Ies2 function as the scaffold (**Fig. 3**) (Tosi et al., 2013). However, exactly how these subunits or subdomains are organized in the 3D space and how the nucleosomal substrate interacts with INO80 remains unclear and controversial.

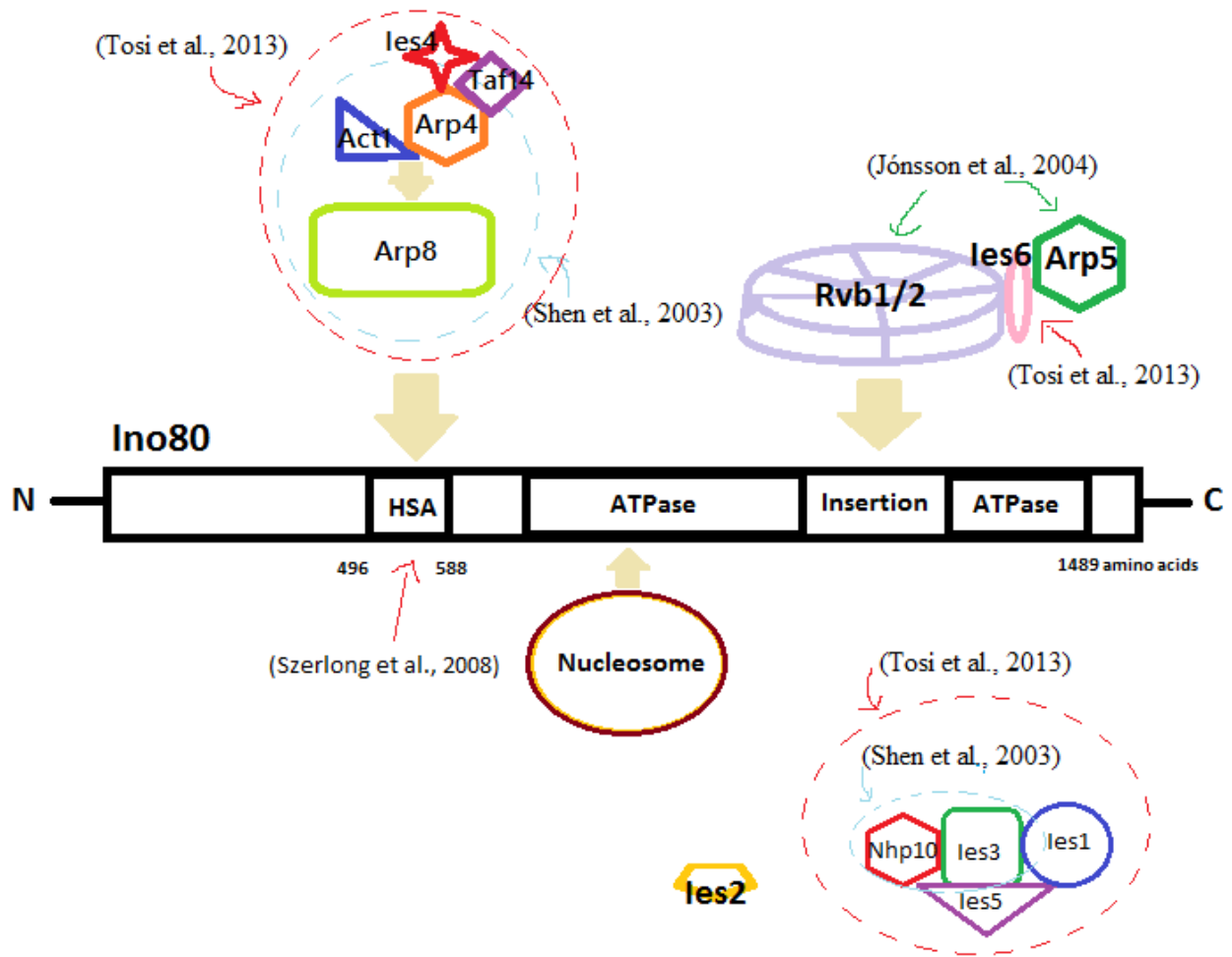


Figure 3. A schematic representation of INO80 organization. INO80 subunits and how they interact with Ino80 polypeptide core subunit are roughly mapped. Ino80 polypeptide chain is 1489 amino acids long, which contains a highly conserved HSA domain (Szerlong et al., 2008) and SF2 Snf2/Swi2 ATPase domain split by an insertion domain. TELY motif, which partially overlaps HSA domain (Kapoor et al., 2013), recruits Arp8, Arp4, and Act1 (not shown). Arp8 forms subdomain with Act1, Arp4, Taf14, and Ies4 (Shen et al., 2003; Tosi et al., 2013). Rvb1 and Rvb2 associate into an individual ring structure before incorporate into INO80 and Rvb1/2 dissociation leads to loss of Arp5 (Jónsson et al., 2004). Ies6 is shown to interact with both Rvb1/2 and Arp5, suggesting its role to connect Rvb1/2 and Arp5 (Tosi et al., 2013). Nhp10 forms subdomain with Ies3, Ies1, and Ies5 (Shen et al., 2003; Tosi et al., 2013).

b. INO80 Subunits

b.1 Ino80

The Ino80 subunit consists of 1489 amino acids and is the catalytic subunit of INO80. Ino80 serves as a scaffold to recruit other subunits. It contains a well-conserved Superfamily 2 (SF2) Snf2/Swi2 ATPase domain. However, unlike the SF2 ATPase domain of many other chromatin remodelers, the ATPase domain of Ino80 is split by a long insertion domain (Watanabe and Peterson, 2010) (**Fig. 3**). Function of this insertion domain remains unknown. Another highly conserved domain within the Ino80 polypeptide is the helicase-SANT-associated (HSA) domain. The HSA domain of another chromatin remodeler, RSC, has been shown to bind the actin related proteins Arp7 and Arp9 with high selectivity (Szerlong et al., 2008). Similarly, the HSA domain

of INO80 –[which was further narrowed down to a TELY motif (residues 531-598)] is important for recruiting the Act1, Arp4 and Arp 8 subunits (Kapoor et al., 2013).

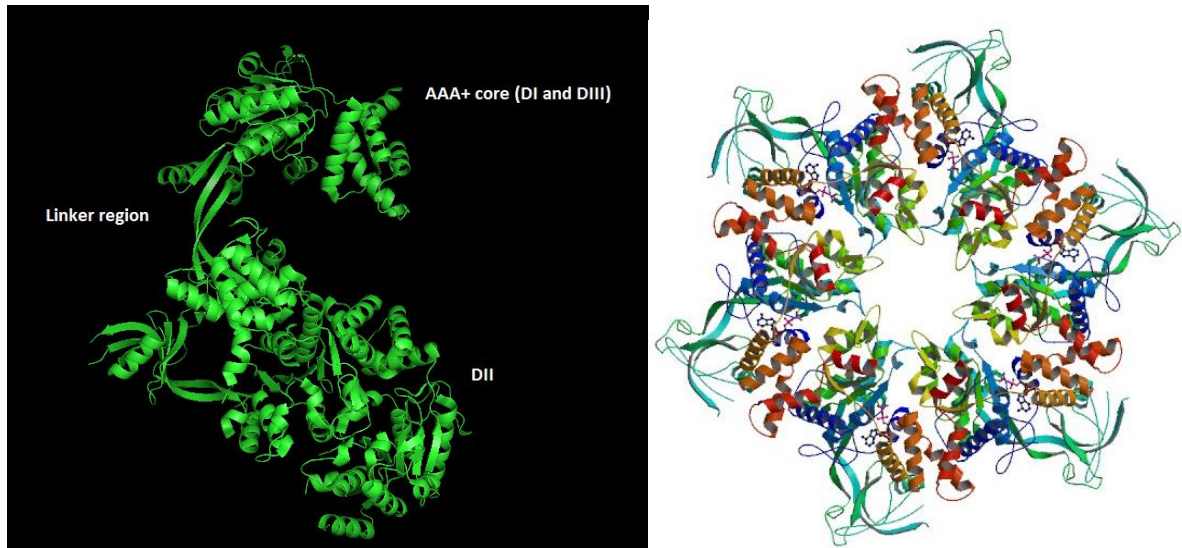
b.2 Actin and ARP

Actin and Actin-related proteins (Arps) are frequently found in chromatin remodeling complexes. Their role in chromatin remodeling remains unclear but they have been shown to interact with histones and modulate the ATPase activity of the remodeler translocase (Szerlong et al., 2008). Arp5 and Arp8 are present exclusively in INO80 and not in other chromatin remodelers (Conaway and Conaway, 2009). In contrast, Arp4 is present in several chromatin remodeling complexes, including SWR1 and NuA4 (Fenn et al., 2011). Arp5 and Arp8 are required for the activity of INO80 and have been shown to bind both DNA and histones (Shen et al., 2003). Inactivation of the *ARP5* and *ARP8* genes exhibit similar phenotype as *ino80Δ* knockout mutant cells, further supporting its functional role in the context of the INO80 complex (Gerhold et al., 2012). Act1 has a minor role in nucleosome mobilization (Kapoor et al., 2013). Arp8 binds to the TELY motif of HSA domain and recruits Arp4 and Act1 (Shen et al., 2003). Arp8 binds all 4 canonical histone proteins, but prefers H3 and H4 (Shen et al., 2003). Arp4 has a higher affinity for H3-H4 dimers over intact nucleosomes (Gerhold et al., 2012). *In vitro*, recombinant Arp8 is dimeric and can form a complex with H3-H4 tetramer. However, biochemical studies of the native INO80 complex suggest that Arp8 exists as a monomer in the context of INO80. One possibility is that Arp8 and Arp4 forms a heterodimer in INO80 to bind the nucleosome (Fenn et al., 2011; Saravanan et al., 2012). However, this model remains to be tested.

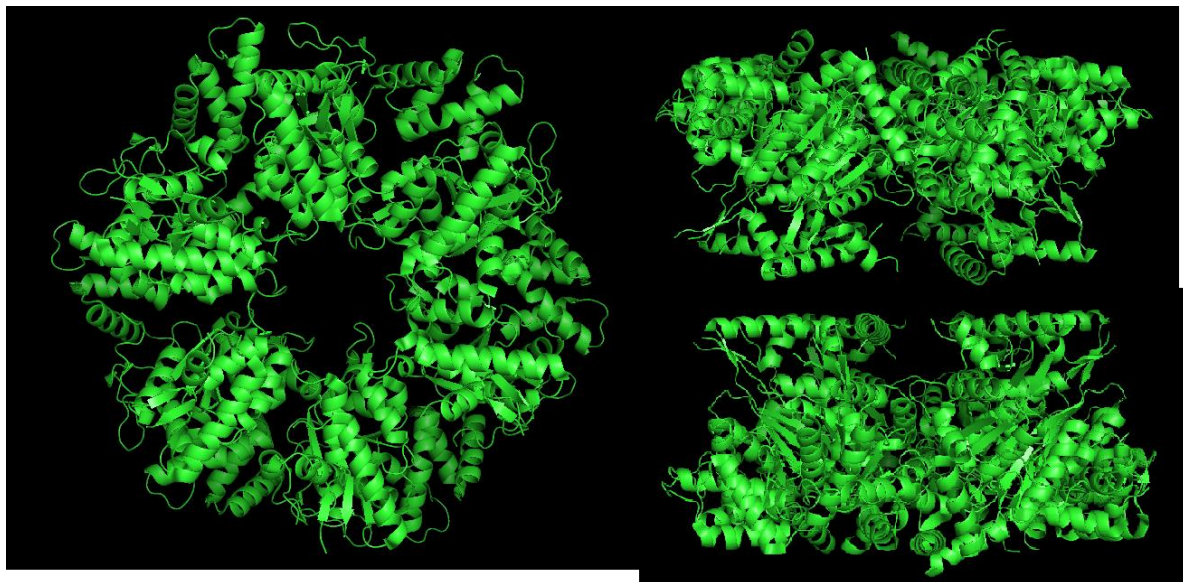
b.3 Rvb1/2

Rvb1 and Rvb2 belong to a large family of proteins called AAA+ ATPase (ATPases Associated with diverse cellular Activities). The Rvb1/2 complex is known as TIP48/49, pontin52/reptin52 and Tih1p/2p in higher eukaryotes. How the yeast Rvb1/2 is involved in the molecular function of INO80 remains unclear. *In vitro*, Rvb1 and Rvb2 individually exist as ring-shaped hexamers with a central pore. When recombinant Rvb1 and Rvb2 fold together, they assemble to form a dodecamer consisting six copies of each protein forming two stacked hexameric rings (Conaway and Conaway, 2009). Each monomer of Rvb1 and Rvb2 consists of 3 domains. Domains 1 and 3 is associated with the AAA+ ATPase, while domain 2 is insertion region that splits the ATPase into two halves. Crystal structures of human Rvb1 hexamer (**Fig. 4a**) (Matias et al., 2006), Rvb1/2 with truncated domain 2 (**Fig. 4b**) (Gorynia et al., 2011), and a cryo-EM structure of yeast Rvb1/2 dodecamer have been reported (**Fig. 4c**) (Torreira et al., 2008).

(a)



(b)



(c)

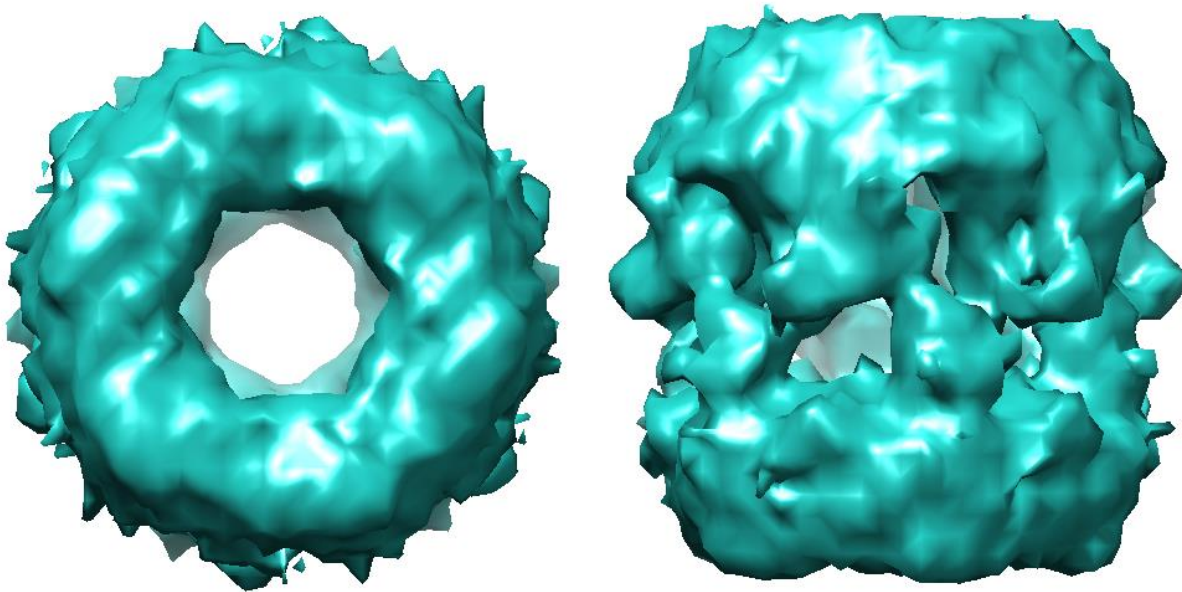


Figure 4. Rvb1/2 Structures. (a) The 2.2 Å crystal structure of human Rvb1 protein is shown as a ribbon representation. It has an AAA+ core (Domain I and III) which is split by the insertion domain (Domain II). Hexameric ring of Rvb1 is shown to the right (PDB ID: 2C9O). (b) Crystal structure of human RuvBL1/2 dodecamer ring (double heterohexamers) with truncated domain II bound to ADP/ATP solved at 3 Å resolution (PDB ID: 2XSZ). (c) Top and side views of surface-rendered cryo-EM map of the yeast Rvb1/2 dodecamer ring determined at 13.6 Å resolution (EMDB ID: 2865).

b.4 Other Subunits

Nhp10 is a non-conserved subunit in yeast and it contains HMG domain, a DNA binding motif. Nhp10 and Ies3 are involved in targeting INO80 to DNA, but do not appear to be required for ATPase activity and remodeling activity of INO80 (Shen et al., 2003). Nhp10 and Ies3 are also involved in a repair response to DNA damage (Clapier and Cairns, 2009). Taf14 contains the YEATS domain at its N-terminal region and is also found in other complexes, including TFIID and SWI/SNF. It is involved in chromatin remodeling as well as transcriptional regulation (Zhang et al., 2011a).

EM Approach to Studying INO80 Structure

The large size (~1.3 MDa) of the multiple-subunit INO80 makes electron microscopy an ideal method to study its structure. Transmission Electron Microscope (TEM) can provide the internal structure information of a 3D object at high resolution (up to a single digit angstrom) by shooting high energy electron beam (100 – 300 kV) through the specimen in an extremely high vacuum environment (~ 1×10^{-6} Pa). EM image can be recorded digitally in a charge coupled device (CCD) camera. An EM image is a 2D projection of the 3D sample modified by an instrument-specific Contrast Transfer Function (CTF). CTF represents the degree of spreading of point object, thus it can indicate the image quality. Correction for CTF effort computationally improves image resolution (**Fig. 5**) (Cong and Ludtke, 2010). Single particle analysis is one of approaches to utilize TEM for structural study. In this approach, the orientation of individual molecules, i.e. their Euler angles, is unknown, and has to be determined computationally. The raw

particle images are noisy and of low contrast; they are aligned and sorted into different classes to generate better-defined class averages. 3D map can then be computed from 2D averages in a back projection scheme (Cong and Ludtke, 2010). This method can reveal conformational heterogeneity of a sample, which was indeed the case for INO80.

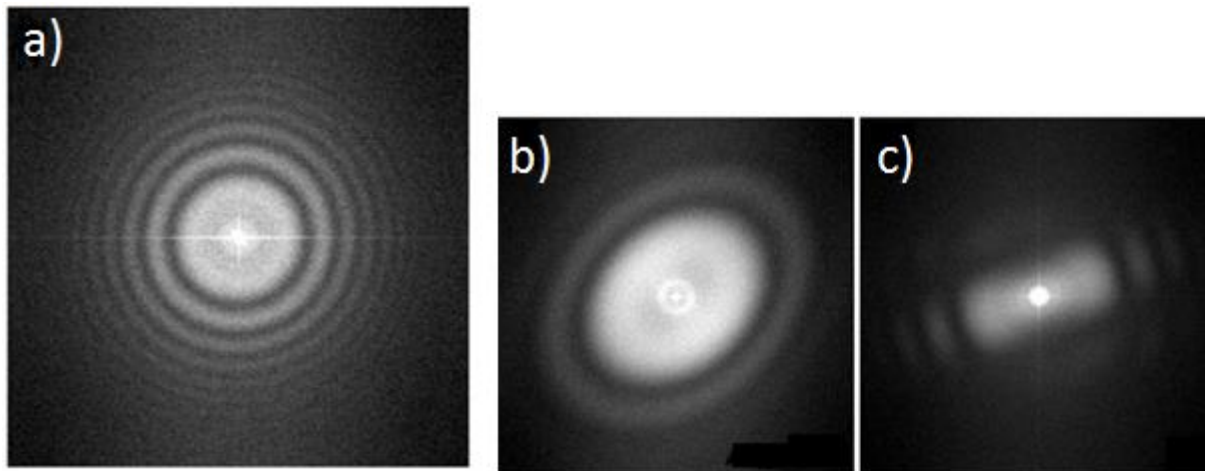


Figure 5. Examples of how CTF demonstrates EM image quality. (a) Symmetric CTF ring indicates absence of astigmatism; EM image is not distorted with optimal contrast. (b) Elongated CTF ring indicates the presence of astigmatism. EM image is distorted. (c) CTF ring is missing in upper and lower regions, indicating specimen drift during electron exposure and image recording.

a. EM Sample Preparation

INO80 sample was prepared by negative staining method as well as vitrification method before being put in an EM. Main purpose of sample preparation was to stabilize INO80 for extremely high vacuum of EM that needs to be maintained in order to avoid electrons scattering before reaching the specimen. In negative staining method, depleted radioactive heavy salt uranyl acetate was used as a staining solution, which surrounds the sample, but excludes density inside. Heavy salt in staining readily interacts with electron beam and produces image contrast. When electron beam passes through the sample, which excludes stain, it creates less deflection than stain-rich regions, thereby producing hollow shape in a darker staining solution (Leschziner, 2011). It can generate high contrast with a high signal-noise ratio. However, heavy salts limit resolution of 3D reconstruction and only the surface or topology of molecule can be defined. Also, dehydration step can distort conformation of sample by flattening its shape (Ohi et al., 2004). Further, incompatible buffer could cause protein aggregations and introduce artifacts.

Specimen vitrification was used in cryo-EM. In our work, purified INO80 sample was pipetted onto a holey carbon film of an EM grid, which was rapidly plunged into cryogen (liquid ethane) in order to freeze sample and suppress the ice crystal formation. Before plunging, the sample droplet was blotted with a piece of filter paper, leaving only a thin layer of its solution on EM grid, ensuring the sample transparent to electron beam (Dobro et al., 2010). Cryo-EM has the advantage of maintaining sample in hydration and in a near native state. Sample is more uniform and less distorted in the near native state. However, cryo-EM image has very low signal-noise ratio because density of sample is only slightly greater than the surrounding thin layer of vitrified ice and only a small electron dose ($10 \text{ e}/\text{\AA}^2$) can be used for exposure to avoid beam-induced damage.

Therefore, it is difficult to distinguish between differently oriented molecules and molecules in different conformations of a conformationally heterogeneous sample.

b. Chemical Fixation

Several factors such as structural heterogeneity, sample aggregation, and buffer incompatibilities limit resolution of 3D reconstruction of INO80 which is composed with multiple subunits. Therefore, chemical fixation was needed to increase conformational and compositional homogeneity of sample for EM analysis. Chemical fixation is less disruptive for preparation methods such as chromatography and dialysis, however directly adding fixing reagent can cause sample aggregation, inter-particle fixation, and introduce artifacts because of low salt concentration (Stark, 2010). GraFix method adds fixing reagent to a density gradient by using glycerol gradient centrifugation (**Fig. 6**) (Stark, 2010). Thus, buffer solution will completely exchange with sample before chemical fixation. The pressure of centrifugation can disrupt weak aggregations and prevent cross-linking between individual macromolecules (Stark, 2010). As a result, macromolecule sample prepared with GraFix has less broken or partial molecule and reduced sample aggregation.

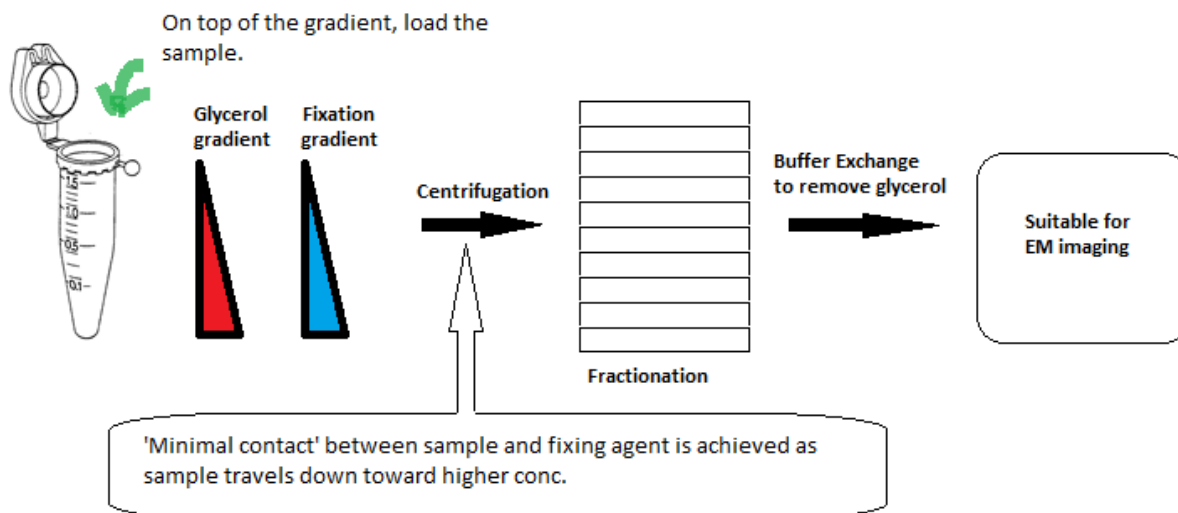


Figure 6. The GraFix method. Gradients of glycerol and fixation reagent generate fractions by centrifugation. Each fraction can be analyzed by EM by removing glycerol through a buffer exchange column (Stark, 2010).

c. Image Alignment

In single particle analysis, orientations and position of individual INO80 particles have five degrees of freedom that would create different projections: two positional parameters (x and y coordinates) in a 2D image and three rotational parameters (ψ , θ , and ϕ) (Heel et al., 1997). Two methods were devised to determine the relative orientations of individual particles in EM images; Angular Reconstruction (AR) and Random Conical Tilt (RCT). AR adopted common lines approach to find a 1D line shared by two different 3D projections of a 3D object in Fourier Transform (FT). Relative Euler angle orientations can be determined by the angles formed between common-line projections and they are used to assign 2D class averages (Heel et al., 1997). AR has a bias limitation which assumes the sample is homogenous in conformation only projected into different orientations (Leschziner, 2011). In RCT, the EM sample is physically tilted to obtain two

views of each molecule, one untilted and the other with a tilt angle (in this study, 50° was used). It allows effective noise discrimination because tilted images of known angle should have a conical tilt series (Frank et al., 1986). However, RCT has missing information of relatively large angle (~80°) because of limited rotation capacity of EM sample holder. Also, shooting electron beam to identical region twice would limit the image resolution by 1) radiation damage of molecules and 2) conformational distortion by electrically charging molecules (Frank et al., 1986).

d. 2D Classification and 3D Reconstruction

After EM images were obtained, individual particles were selected manually on a computer screen. Then, the CTF effect was corrected in order to minimize image distortion induced during EM image formation (Cong and Ludtke, 2010). CTF correction included low pass filtering the particle images to eliminate high frequency noises and phase flipping (by multiplying -1) at specific frequency ranges. Then, an iterative computation procedure was performed on INO80 particle images to generate 2D classifications of different orientations and finally 3D reconstruction model.

Reference-free 2D analysis categorized 2D particles into classes or views of different orientations or conformations by comparing and averaging (Cong and Ludtke, 2010). Based on 2D class averages, a set of low-resolution initial 3D models were generated. Then, initial 3D models were selected, which represent 2D projections of reference-free 2D class averages. They were further refined against raw 2D particles until convergence.

II. Materials and Methods

Sample Preparation

Biochemical works were done by Dr. Lihong Wan of Dr. Ed Luk's group in Stony Brook University. FLAG-tagged INO80 from whole cell extract was purified and chemically fixed by GraFix method (Stark, 2010). Two different crosslinking reagents were used in our studies. Glutaraldehyde was used in the initial phase of the study as it was recommended in the original GraFix protocol developed by (Stark, 2010). However, since the covalent crosslinking of glutaraldehyde is irreversible, we later adopted the use of formaldehyde crosslinking, which is reversible thereby allowing verification of the subunit composition of the sample. Once the sample fractions were gone through the buffer exchange to remove glycerol, I diluted each sample with several concentrations and determined optimal concentration for EM imaging.

Grid Preparation

Two types of grids were used to prepare negative stained EM grid and cryo-EM grid. Meshed grid (SPI Supplies) covered with a carbon layer was suitable for negative stained EM grid since stain can provide high contrast. However, cryo-EM grid has a very low contrast therefore I used the lacey holey grids (SPI Supplies) that contained an additional carbon layer; holes on holey grid can contain solvent which is advantageous for keeping sample hydrated and thin ice layer can evenly spread across the carbon layer. To put a carbon film on grids for supporting the sample, I first placed a sheet or two of freshly cleaved mica (Ted Pella) in a vacuum evaporator (Edwards) and evaporated a thin layer of carbon (~ 10 nm) onto mica from a graphite rod (Ted Pella). Then, I floated the carbon film off the mica surface in deionized water and deposited onto EM grids. After carbon-coated grids were dried, I glow-charged the grids within argon plasma in a vacuum chamber (Edwards) to restore hydrophilicity of carbon films. It allows aqueous sample to spread evenly on the grid and form thin layer when blotted with a piece of filter paper (Dobro et al., 2010).

Sample on Grid

While the EM grids were freshly cleaned, I applied aqueous sample on the grid, blotted, applied 2% depleted uranyl acetate solution 2 -3 times, and air-dried in room temperature for negatively staining EM. For cryo-EM, first I liquefied ethane gas in a cup cooled by liquid nitrogen (~ -175 °C). Next, I performed sample application, blotting, and plunging into cryogen in Vitrobot plunge-freezing advice (FEI) set to 70% relative humidity. High humidity in the chamber generates favorable environment for sample to adhere better to grid by electrostatic force and also prevents sample desiccation before plunging into cryogen. It is very important to prevent sample exposure to moisture in the air while transferring the grid from cryogen to grid storage box as this could lead to the formation of a thick layer of crystalline ice (Dobro et al., 2010).

EM Imaging

INO80 imaging was performed with JEOM 2010F TEM (JEOL) at 200 kV and images were recorded with 50,000x magnification using a 4k x 4k Ultra-Scan 4000 CCD camera (Gatan) which corresponds to 2.12 Å/pixel sampling level. I followed instruction on article by (Sun and Li, 2010) which is specifically written for JEOM 2010F TEM. To prepare the EM operation, I cooled down CCD camera to -25 °C to stabilize the camera and reduce the number of thermal electrons in CCD chip. For negative stained EM, I inserted a grid into a 70° specimen tilt holder

(Gatan), and for cryo-EM, I transferred vitrified grid in liquid nitrogen into a 60° cryo-specimen tilt holder (Gatan). Once the specimen holder was inserted and column vacuum recovered to $\sim 1-3 \times 10^{-5}$ Pa, I aligned microscope; centering FEG, spot size, and correcting objective lens astigmatism. When imaging the sample, I under-focused the objective lens to obtain sufficient contrast of the particles so I could identify them over the background. Frequent re-alignment of the instrument was necessary because of uneven surface and height of grid, specimen drift, charging, and astigmatism. Specimen drift was very common because of mechanical vibration and large mechanical movement of the specimen in order to locate next areas on the grid. Positive charging was also observed which occurs when incidence electrons knock out electrons in specimen. Charging distorts the image and causes uneven electron phase shift. After each image was generated on computer display, I analyzed CTF by calculating a Fourier transform of the acquired image in order to decide whether to save the image for further processing. Then I would adjust parameters and search for a new area for taking next image. In the case of RCT, first I obtained 5-6 tilted images at -50° tilt and I obtained 5-6 images at 0° that corresponded to tilted images.

2D Classification and 3D Reconstruction

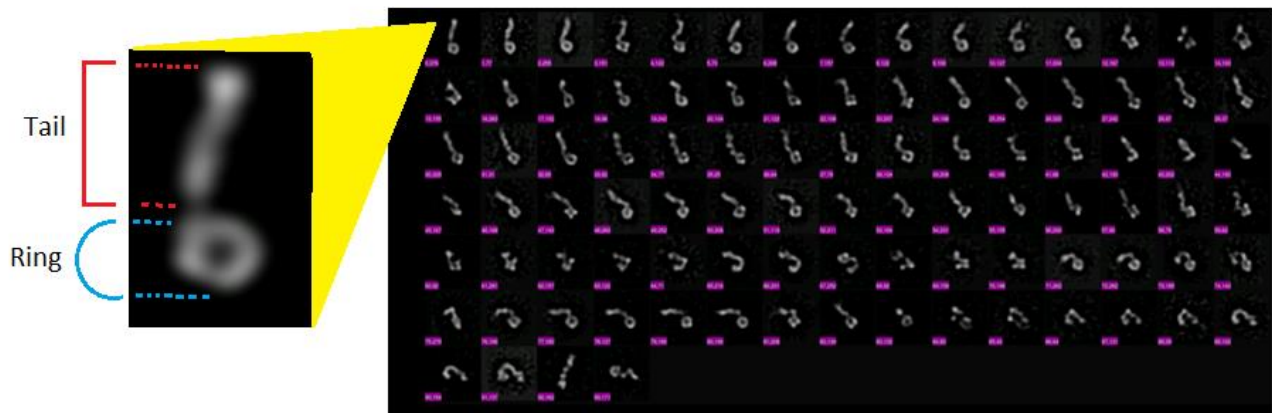
For 2D image processing and 3D model reconstruction of INO80, I used Python-encoded software EMAN (Ludtke et al., 1999) and EMAN2 (Tang et al., 2007) on Linux workstation (DELL). First, I used *e2boxer* in EMAN2 to manually pick particles on contrast-enhanced images (low passed and reduced pixel size to 8.46 Å/pixel). I also attempted picking particles with Swarm mode (semi-automatic) and Gaussian mode (automatic), however they were unsuccessful because INO80 particles are flexible and heterogeneous in conformation. Next, I binned the original images by a factor of 2 to 4.23 Å/pixel sampling level, and used *refine2d.py* in EMAN to generate 2D class averages. I altered a number of expected classes depending on the number of particles in the dataset. Also, I deleted “bad” particles that do not conform to any classes to improve class averages. Once I determined that a set of class averages represent a certain degree of different orientations and conformations, I proceeded to use *e2workflow.py* in EMAN2 to generate initial models. INO80 has asymmetry conformation and a strongly preferred orientation on carbon support film, as a consequence some initial models could be incomplete and misrepresenting. Therefore, I used several initial models for 3D reconstruction with iterative *refine* commands in EMAN. Several parameters were remained constant for different samples; “hard=25”, a criterion value to discriminate against inconsistent class averages, “sym=c1”, c1 indicates no symmetry which I was confident from my observation, and “classkeep=.5”, a coefficient value to exclude noticeably different particles from class averages. Also, script contained Even/Odd test that compares the consistency of two 3D reconstructions calculated from even numbered data and odd numbered data respectively, to estimate the resolution of a 3D reconstruction. In addition, I attempted to use refined 3D model of < 30 Å resolution as an initial model for 3D refinement. I used UCSF Chimera to visualize the 3D EM models, make measurements, and compare with published 3D EM maps (Tosi et al., 2013). To validate the iterative refining steps and estimate the resolution of 3D model, I used FSC algorithm of EMAN. FSC threshold used for assessment was 0.5.

III. Results

WT INO80

First trial of reference-free 2D class averages contained a large number of unverified particles and aggregates of multiple particles, therefore re-selection of particles was needed. In cryo-EM 2D class averages, we identified a rigid Rvb1/2 ring and very flexible tail structure (**Fig. 7a**). Majority of Rvb1/2 ring in INO80 were in top or bottom view rather than side view. Also Rvb1/2 ring clearly shows a pore in the middle. Determining INO80 tail structure was difficult because it was flexible both in conformation and length. However, segments within the flexible tail region are visible. Likewise, NS-EM 2D class averages consistently showed Rvb1/2 ring with top/bottom view most of time (**Fig. 7b**). The basic measurements of INO80 are: Rvb1/2 ring diameter is 123 Å, the pore diameter of the Rvb1/2 ring is 34 Å, and the total length of INO80 is 365 Å. I used several initial models to reconstruct and refine 3D models (**Fig. 8**). Cryo-EM 3D model looked similar to a recently published model which also had flexible tail region (EMDB ID: 2386) (**Fig. S1**) (Tosi et al., 2013). The published data also contained Rvb1/2 ring. However, the authors reported a dodecameric organization (stacked double hexameric rings) EM map (EMDB ID: 2865). However, our own data argued against a dodecameric organization as when I superimposed a double-ring model onto our EM structure, one of the two hexameric rings was not completely aligned (**Fig. S2**). NS-EM 3D model seemed to have hollow structure with missing densities due to lower resolution by staining. WT INO80 sample had intact subunits after buffer exchange for EM preparation (data not shown). I also attempted RCT to generate 2D class averages, but it was not successful because of low particle number (data not shown).

(a) Cryo-EM 2D Class Averages of WT INO80



(b) NS-EM 2D Class Averages of WT INO80

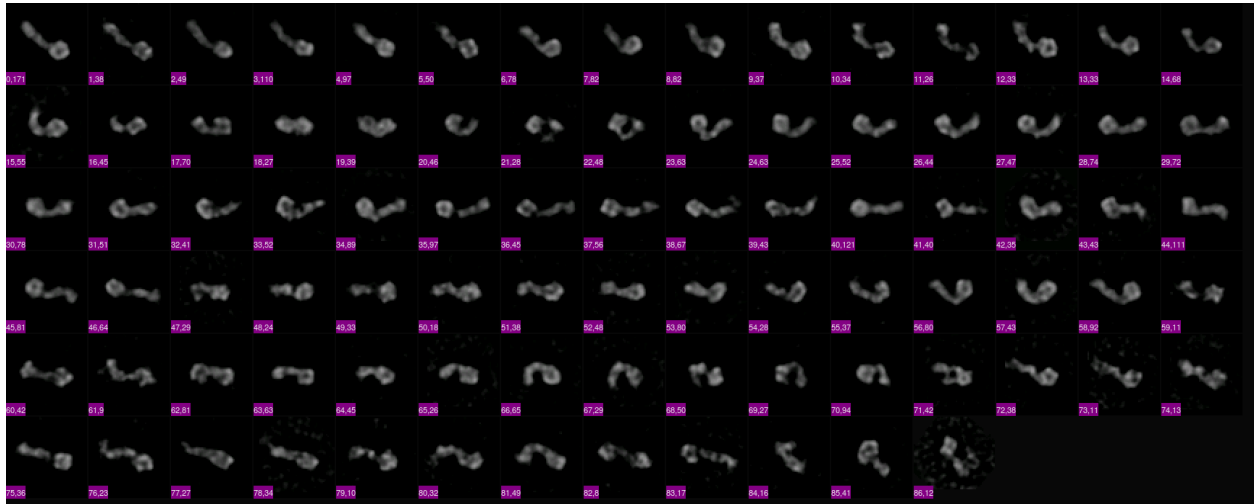
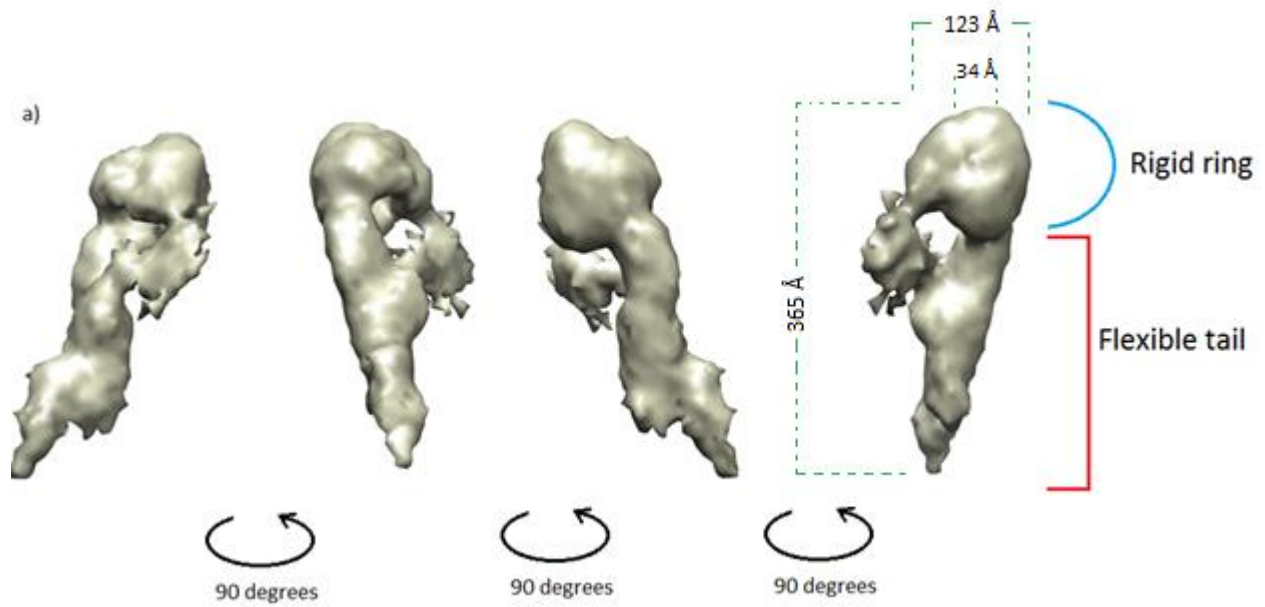


Figure 7. 2D class averages of WT INO80. (a) 94 2D class averages from 15105 cryo-EM particles at 8.46 Å/pixel. (b) 87 2D class averages from 4414 NS-EM particles at 8.46 Å/pixel.



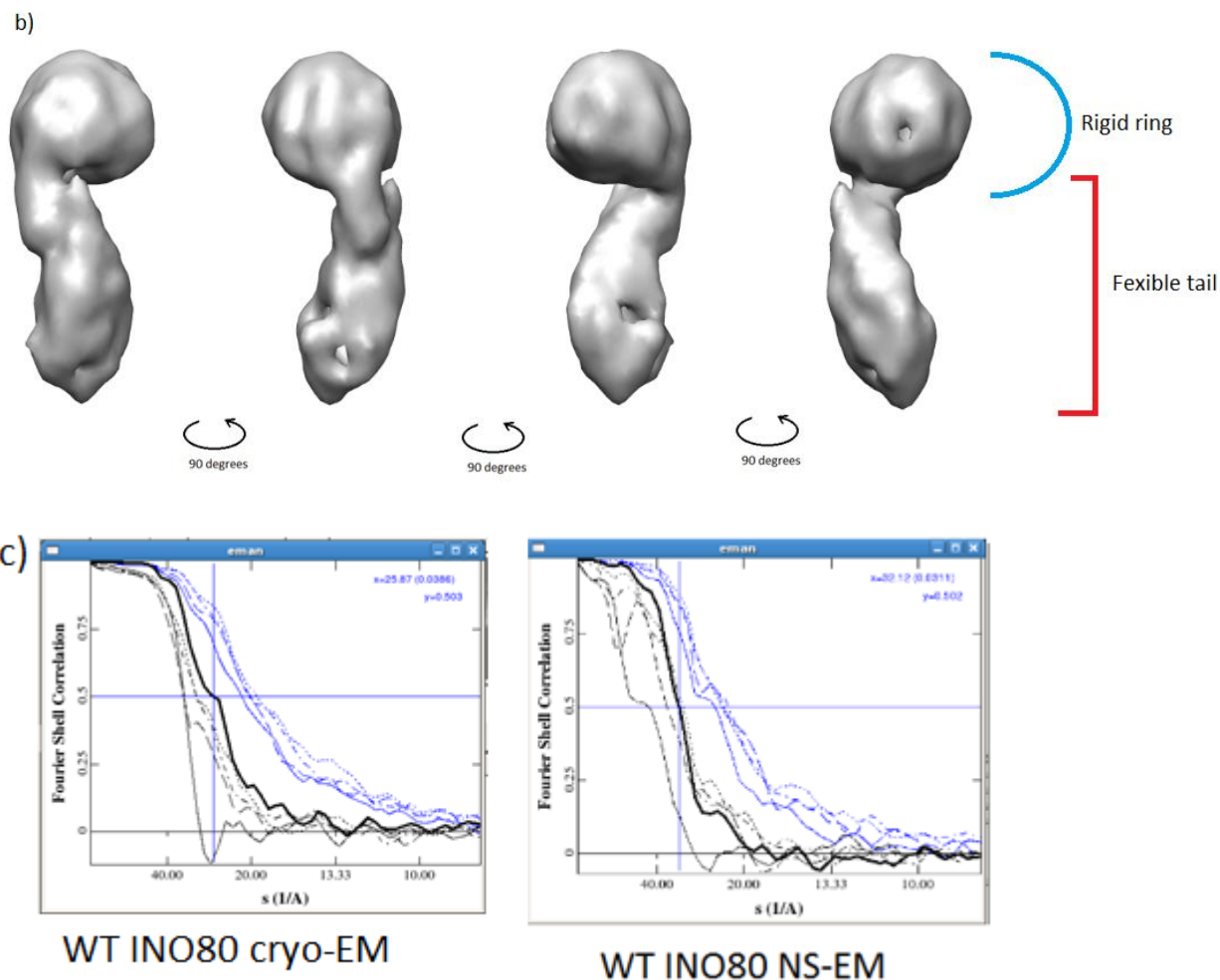


Figure 8. WT INO80 3D models. (a) Cryo-EM 3D model shows a rigid Rvb1/2 ring and a flexible tail with a density sticking out near the Rvb1/2 ring, which is likely an incomplete segment. The identity of the protruding density is unknown. Dimensions of INO80 are shown. (b) NS-EM 3D model has lower resolution with a hollow shape due to missing densities. (c) FSC curves show 25 Å resolution for the WT INO80 cryo-EM 3D model and 32 Å resolution for the NS-EM 3D model.

INO80 with MBP-Labeled Subunits

To determine how Rvb1/2 monomers form ring structure in INO80, INO80 with Rvb1-MBP sample was used. 2D class averages of NS-EM INO80 with Rvb1-MBP shared high similarity with that of WT INO80 (**Fig. 9**) and unfortunately, the difference was very subtle. In order to verify this observation, I generated several 3D models and performed multi-refinement with initial 3D models of WT INO80 (not shown). INO80 with Arp5-MBP sample was prepared with formaldehyde. 2D class averages results were very similar to that of WT INO80 with subtle difference (**Fig. 10**). Before fixation, both fusion complexes with Rvb1-MBP sample and INO80 with Arp5-MBP sample were examined for function and structural integrity (**Fig. S3**).

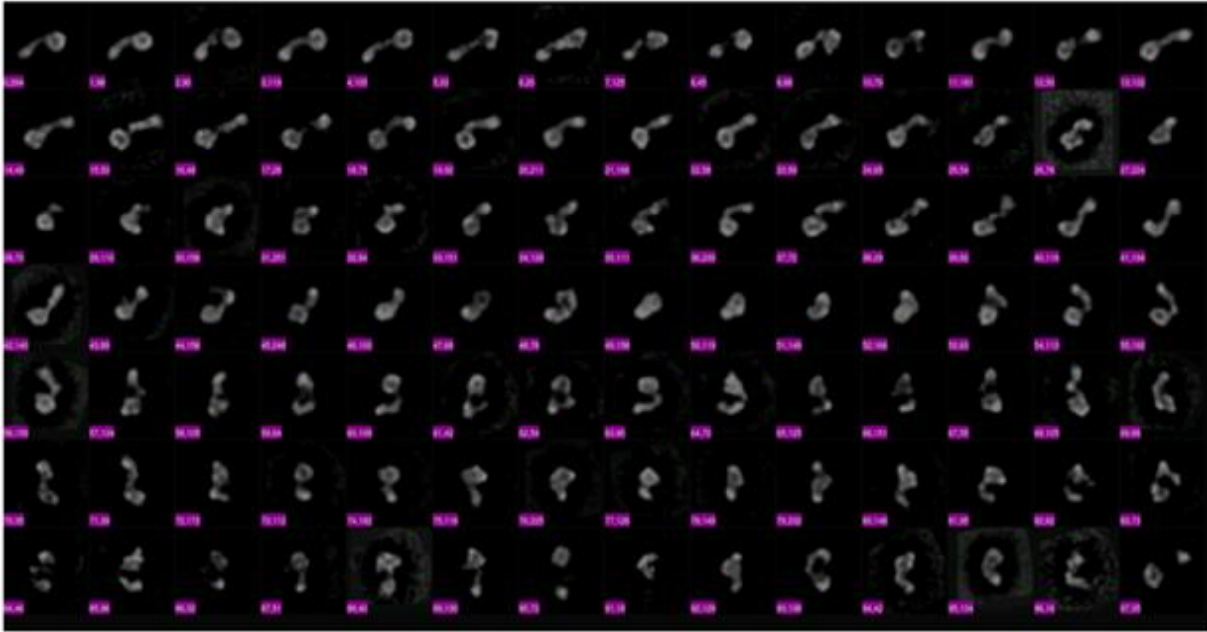


Figure 9. NS-EM 2D class averages of INO80 with Rvb1-MBP. 98 2D class averages from 10439 NS-EM particles at 8.46 Å/pixel. MBP density cannot be identified in these averaged images, likely due to structural heterogeneity of the INO80 complex.

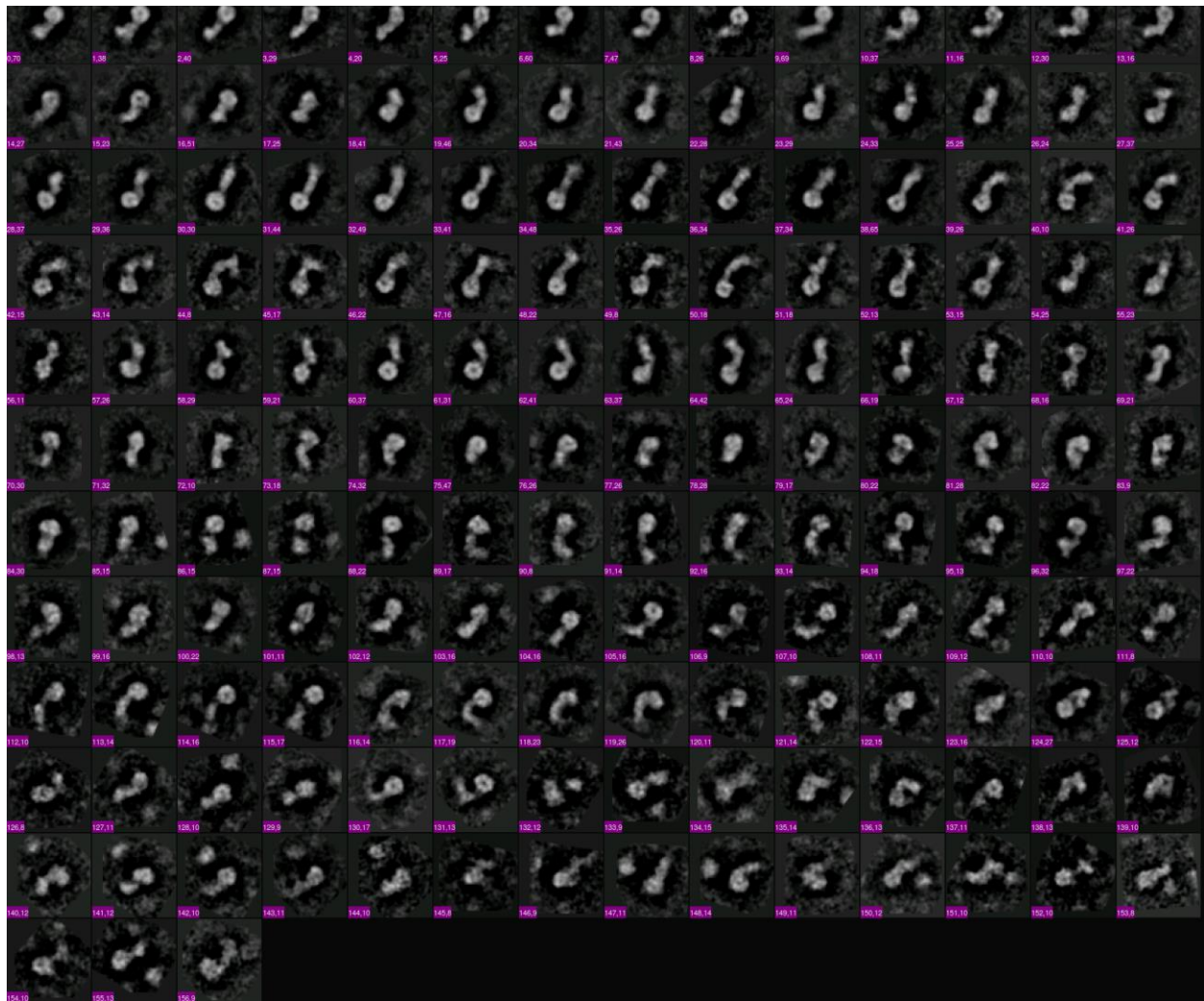
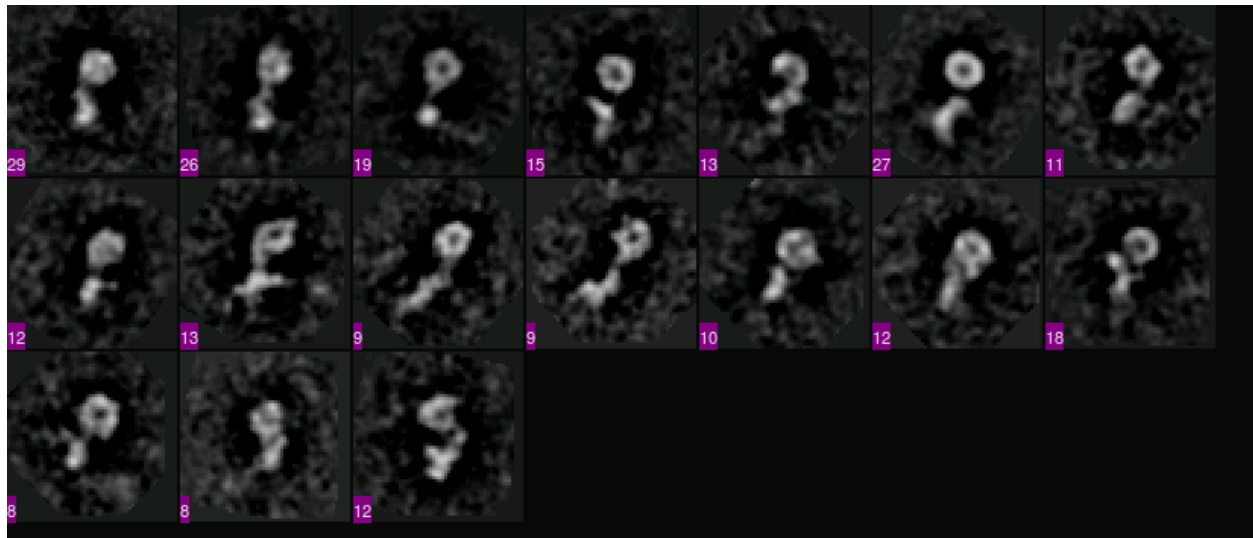


Figure 10. NS-EM 2D class averages of INO80 with Arp5-MBP. 157 2D class averages from 3878 NS-EM particles at 8.46 Å/pixel. MBP density cannot be unambiguously identified in these averages.

INO80 bound to Nucleosome

Sample preparation and EM work of INO80 bound to nucleosome are in progress. Formaldehyde was shown to work equally well as glutaraldehyde for INO80 sample fixation (**Fig. 11**).

(a) NS-EM 2D Class Averages of WT INO80



(b) NS-EM 2D Class Averages of INO80 bound to Nucleosome

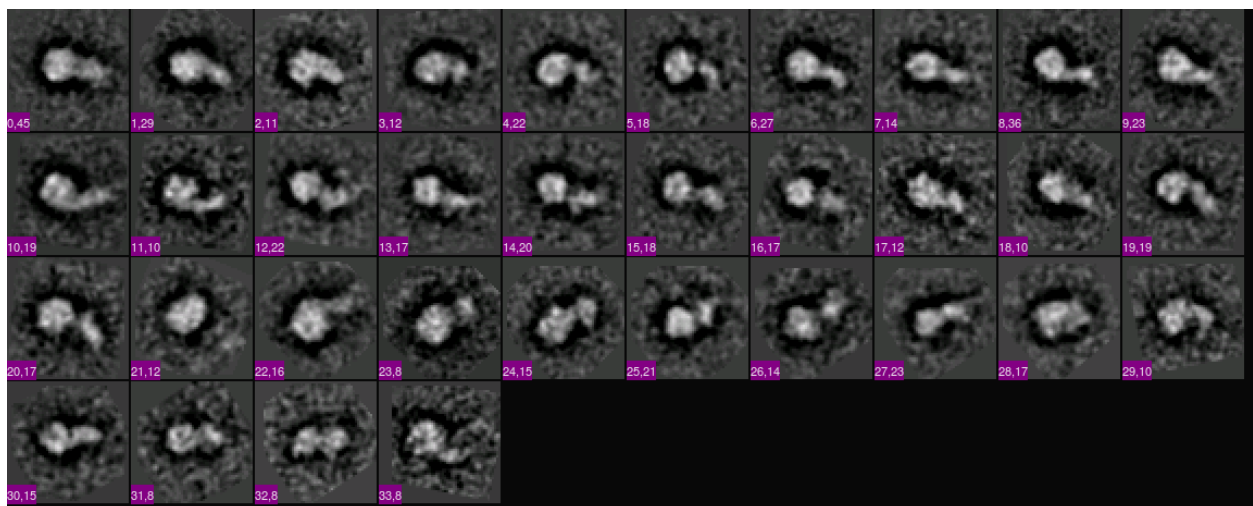


Figure 11. NS-EM 2D class averages of INO80 bound to nucleosome prepared with formaldehyde. **(a)** 17 2D class averages from a small number of NS-EM WT INO80 particles at 8.46 Å/pixel. **(b)** 34 2D class averages from a small number of NS-EM INO80-nucleosome particles at 8.46 Å/pixel.

IV. Discussion and Future Perspective

In this work, we employed electron microscopy to study the structure and conformation of native INO80 from budding yeast. The findings from this INO80 EM study can be summarized as following: (1) We have established a suitable procedure and biochemical condition to isolate and prepare INO80 for EM study; (2) We have revealed the basic architecture of the INO80 complex via 2D image classification and 3D reconstruction. INO80 has a rigid Rvb1/2 ring and a flexible tail region.

From a technical perspective, we determined that the GraFix method was optimal way to prepare INO80 sample for EM imaging. Sample cross-linked this way has in general more homogenous particles and a minimal amount of particle damages and aggregation. Formaldehyde was a competent fixation agent because it could functionally substitute glutaraldehyde and its cross-linking can be reversed. For all samples, Rvb1/2 ring and tail region of various length and conformations (completely looped back, partially folded, and elongated) were present in particles.

We attempted to use a similar approach to analyze the structure of INO80 in complex with the nucleosome. However, our preliminary data did not show extra density that could resemble the nucleosome. One potential problem could be due to non-stoichiometric binding of the nucleosome to INO80. More optimization is necessary to improve the quality of the INO80-nucleosome complexes. To identify the location of individual subunits of INO80, we are systematically fusing the 36 kDa Maltose Binding Protein (MBP) to individual subunit of INO80. This could potentially give positional information for the MBP-tagged subunit on the 3D structure of INO80.

Current study is the first step toward our goal of understanding the INO80 mechanism via structural investigation. Several preliminary results have been obtained so far, although there are lots of work left to be done to improve quality of results. I would like to improve my skill for RCT. MBP fusion strategy has been used successfully for mapping several protein complexes. But this method has not worked for INO80. One possibility is the quality of my INO80 images is not good enough to reveal the subtle density from the small MBP protein (36 kDa). But it is also possible that the highly flexible nature of the INO80 structure has hindered the detection of the MBP density in the averaged images.

V. Supplemental Data

I included recently published 3D EM maps of INO80 (**Fig. S1**) (Tosi et al., 2013) and biochemical data.

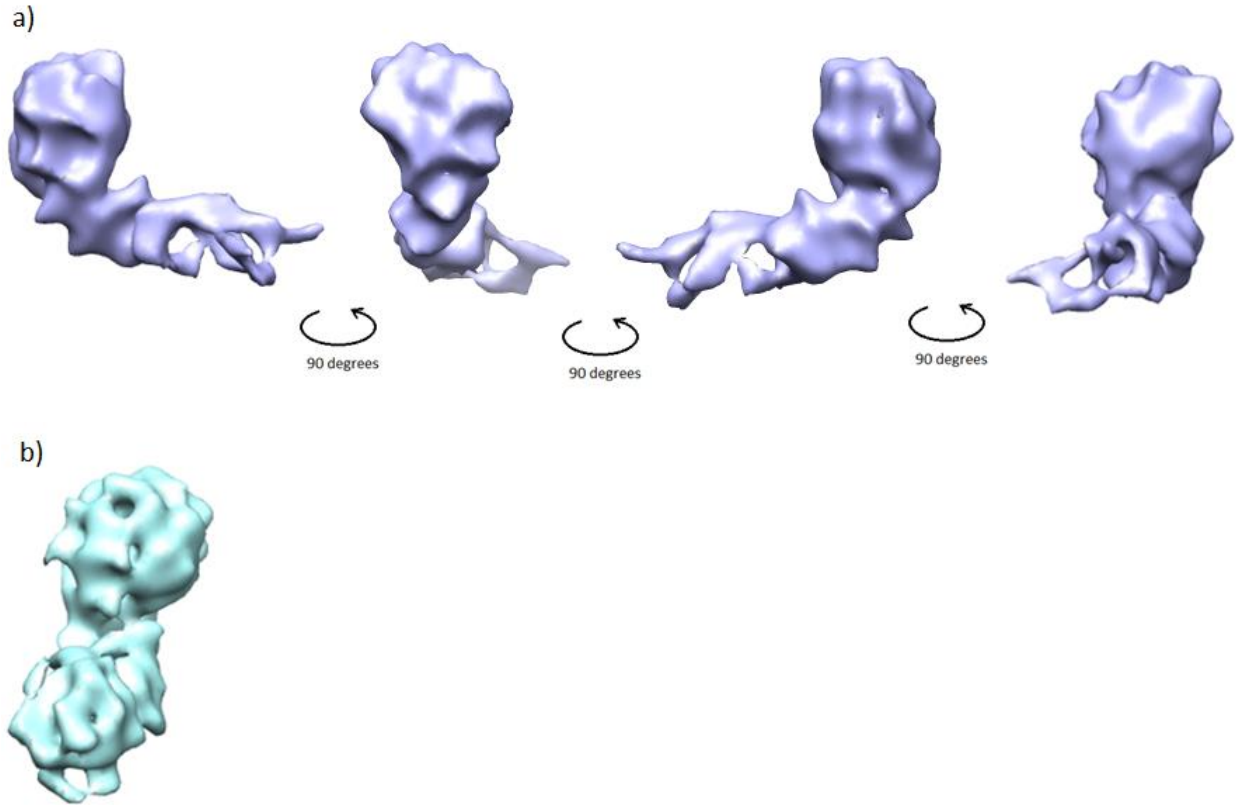


Figure S1. “Embryo-Shaped” INO80 EM 3D maps. (a) WT INO80 cryo-EM 3D model with 13.6 Å resolution in different views (EMDB ID: 2386). **(b)** WT INO80 NS-EM 3D model with 22 Å resolution (EMDB ID: 2385) (Tosi et al., 2013).

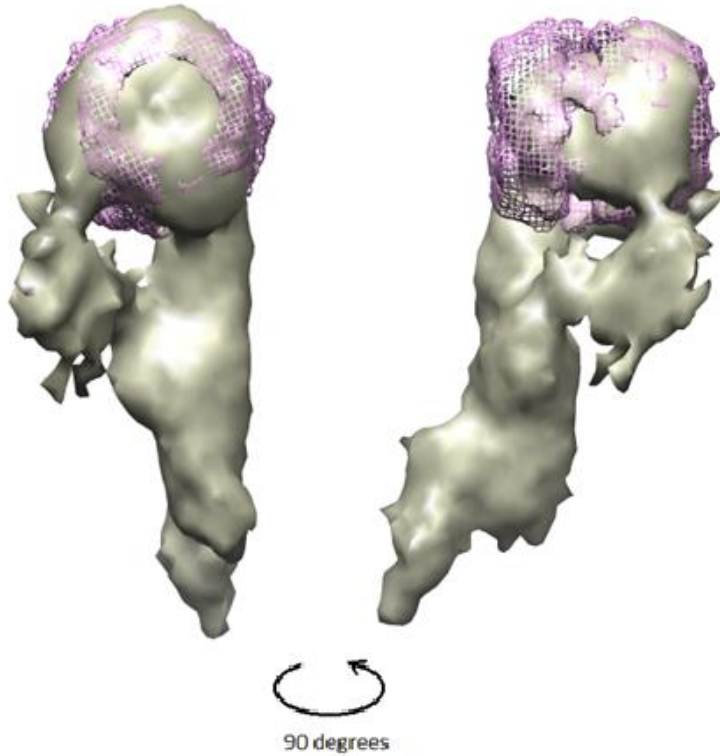


Figure S2. Superposition of cryo-EM structures of WT INO80 and Rvb1/2 dodecamer ring. Ring structure in WT INO80 can roughly occupy single ring of Rvb1/2 dodecamer ring structure (EMDB ID: 2865).

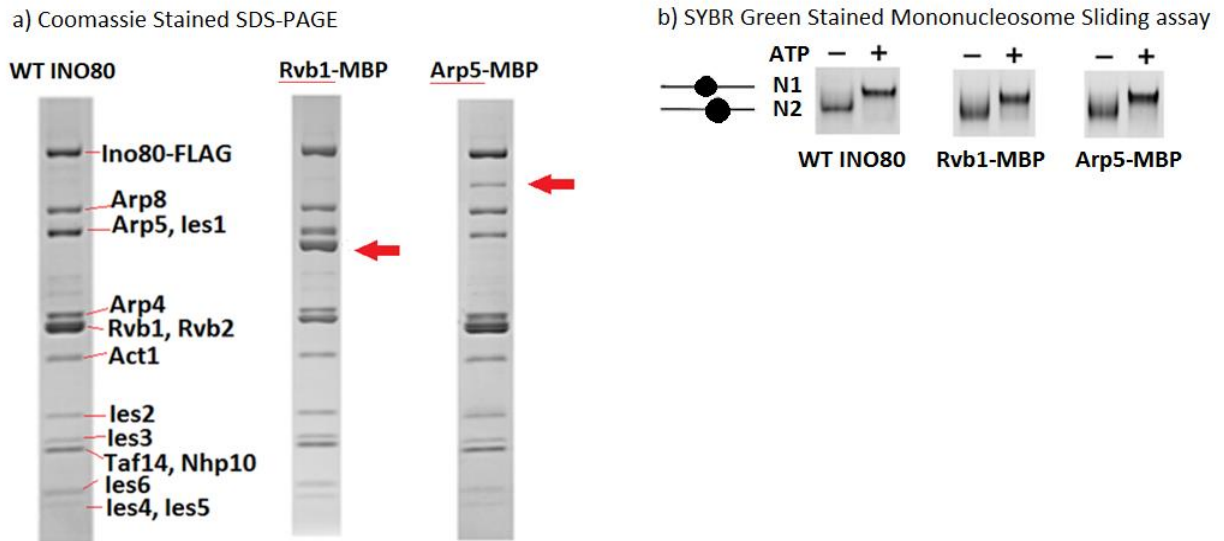


Figure S3. Biochemical data to verify INO80 subunits and function. (a) SDS-PAGE of WT INO80, INO80 with Arp5-MBP, and INO80 with Rvb1-MBP show bands of MBP tagged subunits are shifted and other subunits are present as WT. (b) Mononucleosome sliding-assay of INO80 with MBP tagged subunits shows shifted nucleosome bands.

References

- Bowman, G.D. (2010). Mechanisms of ATP-dependent nucleosome sliding. *Curr. Opin. Struct. Biol.* *20*, 73–81.
- Clapier, C.R., and Cairns, B.R. (2009). The biology of chromatin remodeling complexes. *Annu. Rev. Biochem.* *78*, 273–304.
- Conaway, R.C., and Conaway, J.W. (2009). The INO80 chromatin remodeling complex in transcription, replication and repair. *Trends Biochem. Sci.* *34*, 71–77.
- Cong, Y., and Ludtke, S.J. (2010). Single particle analysis at high resolution. *Methods Enzymol.* *482*, 211–235.
- Dobro, M.J., Melanson, L.A., Jensen, G.J., and McDowell, A.W. (2010). Plunge freezing for electron cryomicroscopy. *Methods Enzymol.* *481*, 63–82.
- Fenn, S., Breitsprecher, D., Gerhold, C.B., Witte, G., Faix, J., and Hopfner, K.-P. (2011). Structural biochemistry of nuclear actin-related proteins 4 and 8 reveals their interaction with actin. *EMBO J.* *30*, 2153–2166.
- Frank, J., Radermacher, M., Wagenknecht, T., and Verschoor, A. (1986). A new method for three-dimensional reconstruction of single macromolecules using low-dose electron micrographs. *Ann. N. Y. Acad. Sci.* *483*, 77–87.
- Gerhold, C.B., Winkler, D.D., Lakomek, K., Seifert, F.U., Fenn, S., Kessler, B., Witte, G., Luger, K., and Hopfner, K.-P. (2012). Structure of Actin-related protein 8 and its contribution to nucleosome binding. *Nucleic Acids Res.* *40*, 11036–11046.
- Gorynia, S., Bandejas, T.M., Pinho, F.G., McVey, C.E., Vornrhein, C., Round, A., Svergun, D.I., Donner, P., Matias, P.M., and Carrondo, M.A. (2011). Structural and functional insights into a dodecameric molecular machine - the RuvBL1/RuvBL2 complex. *J. Struct. Biol.* *176*, 279–291.
- Han, M., and Grunstein, M. (1988). Nucleosome loss activates yeast downstream promoters in vivo. *Cell* *55*, 1137–1145.
- Heel, M.V., Orlova, E.V., Harauz, G., Stark, H., Dube, P., Zemlin F, and Schatz, M. (1997). Angular reconstruction in three-dimensional electron microscopy: historical and theoretical aspects. *Scanning Microsc.* *11*, 195-210.
- Jiang, C., and Pugh, B.F. (2009). A compiled and systematic reference map of nucleosome positions across the *Saccharomyces cerevisiae* genome. *Genome Biol.* *10*, R109.
- Jin, J., Cai, Y., Yao, T., Gottschalk, A.J., Florens, L., Swanson, S.K., Gutiérrez, J.L., Coleman, M.K., Workman, J.L., Mushegian, A., et al. (2005). A mammalian chromatin remodeling complex with similarities to the yeast INO80 complex. *J. Biol. Chem.* *280*, 41207–41212.

- Jónsson, Z.O., Jha, S., Wohlschlegel, J.A., and Dutta, A. (2004). Rvb1p/Rvb2p recruit Arp5p and assemble a functional Ino80 chromatin remodeling complex. *Mol. Cell* *16*, 465–477.
- Kapoor, P., Chen, M., Winkler, D.D., Luger, K., and Shen, X. (2013). Evidence for monomeric actin function in INO80 chromatin remodeling. *Nat. Struct. Mol. Biol.* *20*, 426–432.
- Leschziner, A.E. (2011). Electron microscopy studies of nucleosome remodelers. *Curr. Opin. Struct. Biol.* *21*, 709–718.
- Ludtke, S.J., Baldwin, P.R., and Chiu, W. (1999). EMAN: semiautomated software for high-resolution single-particle reconstructions. *J. Struct. Biol.* *128*, 82–97.
- Matias, P.M., Gorynia, S., Donner, P., and Carrondo, M.A. (2006). Crystal structure of the human AAA+ protein RuvBL1. *J. Biol. Chem.* *281*, 38918–38929.
- Morrison, A.J., and Shen, X. (2009). Chromatin remodelling beyond transcription: the INO80 and SWR1 complexes. *Nat. Rev. Mol. Cell Biol.* *10*, 373–384.
- Ohi, M., Li, Y., Cheng, Y., and Walz, T. (2004). Negative Staining and Image Classification - Powerful Tools in Modern Electron Microscopy. *Biol. Proced. Online* *6*, 23–34.
- Rando, O.J., and Winston, F. (2012). Chromatin and transcription in yeast. *Genetics* *190*, 351–387.
- Saravanan, M., Wuerges, J., Bose, D., McCormack, E.A., Cook, N.J., Zhang, X., and Wigley, D.B. (2012). Interactions between the nucleosome histone core and Arp8 in the INO80 chromatin remodeling complex. *Proc. Natl. Acad. Sci. U. S. A.* *109*, 20883–20888.
- Shen, X., Ranallo, R., Choi, E., and Wu, C. (2003). Involvement of actin-related proteins in ATP-dependent chromatin remodeling. *Mol. Cell* *12*, 147–155.
- Stark, H. (2010). GraFix: stabilization of fragile macromolecular complexes for single particle cryo-EM. *Methods Enzymol.* *481*, 109–126.
- Sun, J., and Li, H. (2010). How to operate a cryo-electron microscope. *Methods Enzymol.* *481*, 231–249.
- Szerlong, H., Hinata, K., Viswanathan, R., Erdjument-Bromage, H., Tempst, P., and Cairns, B.R. (2008). The HSA domain binds nuclear actin-related proteins to regulate chromatin-remodeling ATPases. *Nat. Struct. Mol. Biol.* *15*, 469–476.
- Tang, G., Peng, L., Baldwin, P.R., Mann, D.S., Jiang, W., Rees, I., and Ludtke, S.J. (2007). EMAN2: an extensible image processing suite for electron microscopy. *J. Struct. Biol.* *157*, 38–46.
- Torreira, E., Jha, S., López-Blanco, J.R., Arias-Palomo, E., Chacón, P., Cañas, C., Ayora, S., Dutta, A., and Llorca, O. (2008). Architecture of the pontin/reptin complex, essential in the assembly of several macromolecular complexes. *Struct. Lond. Engl.* *1993* *16*, 1511–1520.

Tosi, A., Haas, C., Herzog, F., Gilmozzi, A., Berninghausen, O., Ungewickell, C., Gerhold, C.B., Lakomek, K., Aebersold, R., Beckmann, R., et al. (2013). Structure and subunit topology of the INO80 chromatin remodeler and its nucleosome complex. *Cell* 154, 1207–1219.

Watanabe, S., and Peterson, C.L. (2010). The INO80 Family of Chromatin-Remodeling Enzymes: Regulators of Histone Variant Dynamics. *Cold Spring Harb. Symp. Quant. Biol.* 75, 35–42.

Whitehouse, I., Rando, O.J., Delrow, J., and Tsukiyama, T. (2007). Chromatin remodelling at promoters suppresses antisense transcription. *Nature* 450, 1031–1035.

Zhang, W., Zhang, J., Zhang, X., Xu, C., and Tu, X. (2011a). Solution structure of the Taf14 YEATS domain and its roles in cell growth of *Saccharomyces cerevisiae*. *Biochem. J.* 436, 83–90.

Zhang, Z., Wippo, C.J., Wal, M., Ward, E., Korber, P., and Pugh, B.F. (2011b). A packing mechanism for nucleosome organization reconstituted across a eukaryotic genome. *Science* 332, 977–980.